



Lake Ice Thickness

D2 (Technical Note): Algorithm Theoretical Basis Document (ATBD)

Reference: CCI-LAKES-0067-ATBD

Issue: 1.1

Date: 11 November 2021

Version history:			
Issue:	Date:	Reason for change:	Author
1.0	13 September 2021	Initial Version	C. Duguay et al.
1.1	11 November 2021	Revision following ESA review	C. Duguay

People involved in this issue:			Signature
Authors:	Claude Duguay	H2O Geomatics	
	Anna Mangilli Pierre Thibaut	CLS	
	Elena Zakharova	Eola	
	Alexei Kouraev	LEGOS	
Internal review:	Stefan Simis	Plymouth Marine Laboratory	
Approved by:	Bruno Coulon	CLS	
Authorized by:	Clément Albergel	ESA	

Distribution:		
Company	Names	Contact Details
ESA	C. Albergel	clement.albergel@esa.int
BC	K. Stelzer	kerstin.stelzer@brockmann-consult.de
CLS	B. Coulon B. Calmettes A. Mangilli P. Thibaut	bcoulon@groupcls.com bcalmettes@groupcls.com amangilli@groupcls.com pthibaut@groupcls.com
CNR	C. Giardino M. Pinardi	giardino.c@irea.cnr.it pinardi.m@irea.cnr.it
Eola	E. Zakharova	zavocado@gmail.com
GeoEcoMar	A. Scrieciu	albert.scrieciu@geoecomar.ro
H2OG	C. Duguay Y. WU	claudeduguay@h2ogeomatics.com mark.wu@h2ogeomatics.com
LEGOS	J.F. Crétaux A. Kouraev	jean-francois.cretaux@legos.obs-mip.fr alexei.kouraev@legos.obs-mip.fr
NORCE	E. Malnes	eirik.malnes@norcere.no
PML	S. G. H. Simis	stsi@pml.ac.uk
SERTIT	H. Yésou	herve.yesou@unsitra.fr
TRE-ALTAMIRA	P. Blanco	Pablo.blanco@tre-altamira.com
UoR	C. Merchant L. Carrea	c.j.merchant@reading.ac.uk l.carrea@reading.ac.uk
UoS	A. Tyler E. Spyraeos	a.n.tyler@stir.ac.uk evangelos.spyrakos@stir.ac.uk

List of Contents

1. Summary	5
2. Introduction	6
3. Algorithm Based on Radar Backscatter and Brightness Temperature	7
3.1. Description.....	7
3.2. Algorithm Definition	9
3.2.1. Ice phenology dates definition algorithm	10
3.2.2. LIT retrieval	10
3.2.3. LIT retrievals editing	11
3.3. Input Data	12
3.3.1. Satellite altimeter backscatter measurements	12
3.3.2. Satellite altimeter brightness temperature measurements	13
3.3.3. CLIMo LIT simulations	13
3.3.1. MODIS/Terra Corrected Reflectance images	13
3.4. Output Data	13
3.5. Quality Assessment	14
4. Algorithm Based on Radar Waveforms	15
5. References	20

1. Summary

This document provides a description of the bases of two novel algorithms for the retrieval of lake ice thickness (LIT) and products generation using data from altimetry missions. The document covers the details required for users to gain an informed understanding of the technical and scientific considerations underlying these products, ranging from the scientific description to functional (inputs, outputs) and mathematical definitions of the algorithms. Both algorithms show good potential for the estimation of LIT, an essential climate variable (ECV) not currently covered in the lakes_cci baseline product generation.

2. Introduction

Lake ice is a major landscape feature in the winter season at northern latitudes and plays a key role in climate moderation and the energy balance (Brown and Duguay, 2010). Lake ice conditions, particularly the length of the ice season and ice thickness, have a significant impact on the economy of northern regions through their influence on transportation, travel, fishing, and recreation activities (Ghiasi et al., 2020). Therefore, accurate knowledge about lake ice properties, such as lake ice thickness (LIT), is necessary. Furthermore, LIT is a key climate change indicator recognized as one of six thematic variables under the GCOS Essential Climate Variable (ECV) Lake. LIT integrates changes in surface air temperature and on-ice snow mass (depth and density) (Brown and Duguay, 2011). Decreasing trends in maximum (late winter) ice thickness have been documented in recent years for lakes on the North Slope of Alaska (ca. 20 cm 1991-2011; Surdu et al., 2014) and in Russia (10-15% decrease 1980-2010; Vuglinsky, 2017).

A limited number of remote sensing investigations have shown the potential of passive microwave, thermal infrared, and active microwave (SAR and altimetry) data for estimating LIT. Kang et al. (2014) found the temporal evolution of Tb measurements from AMSR-E at 10.7 GHz and 18.7 GHz frequency (V polarization) during the ice growth season to be strongly related to ice thickness (Great Bear Lake and Great Slave Lake, Canada). The authors proposed simple linear regression equations to estimate LIT for the lakes using 18.7 GHz V-pol data (2002-2009) with mean bias error (MBE) of 0.06 m and root mean square error (RMSE) of 0.19 m when compared to in situ measurements. Lake surface (ice/snow) temperature observations from MODIS have also been evaluated for estimating lake ice thickness (Kheyrollah Pour et al., 2017). Using heat balance terms derived from the Canadian Lake Ice Model (CLIMo; Duguay et al., 2003), the authors retrieved ice thicknesses up to 1.7 m from MODIS with RMSE of 0.17 m and MBE of 0.07 m when compared to field measurements acquired on Great Slave Lake and Baker Lake, Canada. Murfitt et al. (2018) evaluated RADARSAT-2 C-band synthetic aperture radar (SAR) data for estimating LIT in Central Ontario, Canada. They reported RMSE values of 0.12 m and attributed the uncertainty to unexplored questions about scattering mechanisms and the interaction of the radar signal with mid-latitude lake ice. A recent study by Murfitt and Duguay (2021) further supports the fact that the evolution of backscatter from C-band imaging SAR can largely be explained by an increase at the ice-water interface during the ice growth period and not LIT. Finally, Beckers et al. (2017) explored waveforms from CryoSat-2 Ku-band radar altimetry to estimate LIT on Great Bear Lake and Great Slave Lake. The study reports ice thickness estimates with RMSE of 0.33 m when compared to in-situ measurements made in Back Bay on Great Slave Lake, a site that is located several tens of km away from the CryoSat-2 tracks and not experiencing the same snow and ice conditions. Overall, work on the estimation of LIT from satellite remote sensing is still in its infancy.

This document contains a detailed description of two novel algorithms for the retrieval of LIT using data from altimetry missions. The first algorithm (empirically-based) uses both backscatter (radar altimeter) and brightness temperature (passive microwave radiometer) measurements for the estimation of LIT, while the second algorithm (physically-based) is founded on the exploitation of radar waveforms (Low Resolution Mode). The mathematical formulations, processing steps, input and output data as well as statistical metrics used for quality assessment/validation of each algorithm are provided in the next two sections.

3. Algorithm Based on Radar Backscatter and Brightness Temperature

The algorithm is based on the use of altimetric radar backscatter and brightness temperature, simultaneously measured at nadir on the same satellite platform. This algorithm is fully empirical and requires a calibration step. The algorithm consists of two modules. The first module is dedicated to the determination of ice phenology dates (ice appearance and melt) while the second module is aimed at estimating LIT when ice is present.

3.1. Description

The lake ice phenology dates algorithm has been developed and validated at LEGOS in 2003-2015 (Kouraev et al., 2003, 2004, 2007a,b, 2008a,b, 2015; Kouraev, 2004). This algorithm has been applied to several saltwater seas (Caspian and Aral) and freshwater lakes (Ladoga, Onega and Baikal). The algorithm draws from the synergy of passive and active microwave satellite data - simultaneous active (radar altimeter) and passive (radiometer) observations available from various satellite altimetry missions (TOPEX/Poseidon, Jason-1,-2, ENVISAT, Geosat Follow-On and SARAL/AltiKa).

The method is based on the analysis of the spatio-temporal evolution of two parameters: 1) the altimeter backscatter coefficient (σ_0); and 2) an average value of the brightness temperature at two frequencies (TB/2). The backscatter coefficient is the ratio between the power reflected from the surface and the incident power emitted by the onboard radar altimeter, expressed in decibels (dB). The backscatter at Ku-band (13.6 GHz) is usually used. The second parameter is the average value of the brightness temperature at two frequencies (such as 18 and 37 GHz for T/P and Jason; 23.8 and 36.5 GHz for ENVISAT, etc.). For nadir-looking instruments, open water has a low backscatter coefficient and low brightness temperature values, while ice cover is characterised by a high backscatter coefficient and elevated brightness temperatures.

The distribution of altimetric observations in the space of backscatter versus TB/2 is presented in Figure 1. A cluster marked A with low backscatter coefficient (about 7 dB) and low brightness temperature (TB/2 about 152 °K) represents open water. At the beginning of the freezing period, the formation of young ice brings some observations with high (25-35) backscatter but still low TB/2. Further ice thickening leads to the formation of a cluster of observations (cluster B) characterised by high backscatter coefficient (mainly 15-25 dB) and high brightness temperatures (TB/2 about 230-250 °K). Once the ice starts growing, it gets thicker and more rigid. Wind and currents lead to ice deformation, formation of cracks and ridging, which increases the surface roughness. Snow accumulates, preferentially near the roughest surfaces. All these processes change the dielectric properties of the ice and thus the microwave signal. In general, ice growth, roughening and snow cover on ice lead to decrease of backscatter to 15-20 dB (Ulaby et al., 1986), while TB/2 slightly increases (area between clusters B and C). At the end of the ice season, an ice transformation (melting/refreezing) change the ice surface properties and can result in a backscatter drop of 5-10 dB and slightly increasing TB/2 values (see left limits of cluster C). The formation of melt ponds denotes the beginning ice cover decay and backscatter and TB/2 return to values close to those typical for young ice (right limits of cluster B).

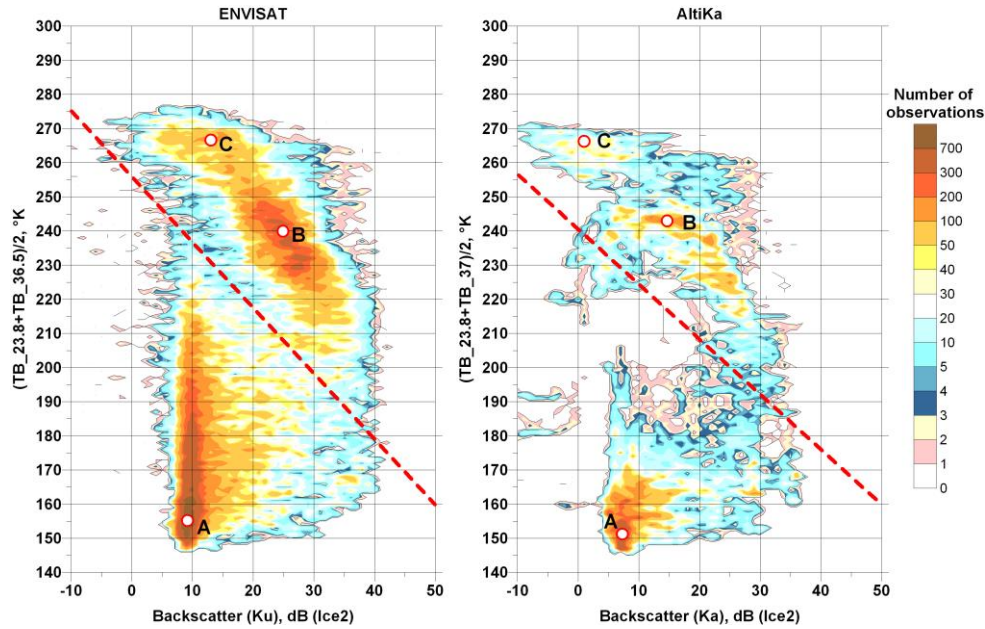


Figure 1. Two-dimensional histograms (number of observations) of ENVISAT and SARAL data for Lake Baikal in the space of backscatter coefficient (Ka or Ku bands) versus the TB/2 (average value of brightness temperature at two frequencies) (Kouraev et al., 2015).

During ice growth, the value of radar altimeter backscatter decreases (Figure 2). This can be explained by the volumetric scattering/absorption of the radar signal within thickening ice. The backscatter decrease is proportional to the ice thickness (Duguay et al., 2018; Zakharova et al., 2020). At Ku-band, the penetration depth into dry freshwater ice is in the order of 5-12 m and depends on temperature and properties of the ice (Legrésy and Rémy, 1997). Therefore, in the case of thin lake ice, the penetration depth for waves emitted at altimetric radar frequencies (C and Ku-band) allows for the estimation of ice thickness.

The brightness temperatures at 18 GHz measured at nadir angle by radiometers installed on altimetric missions also demonstrate a good sensitivity to growing lake ice and can be used for LIT retrievals.

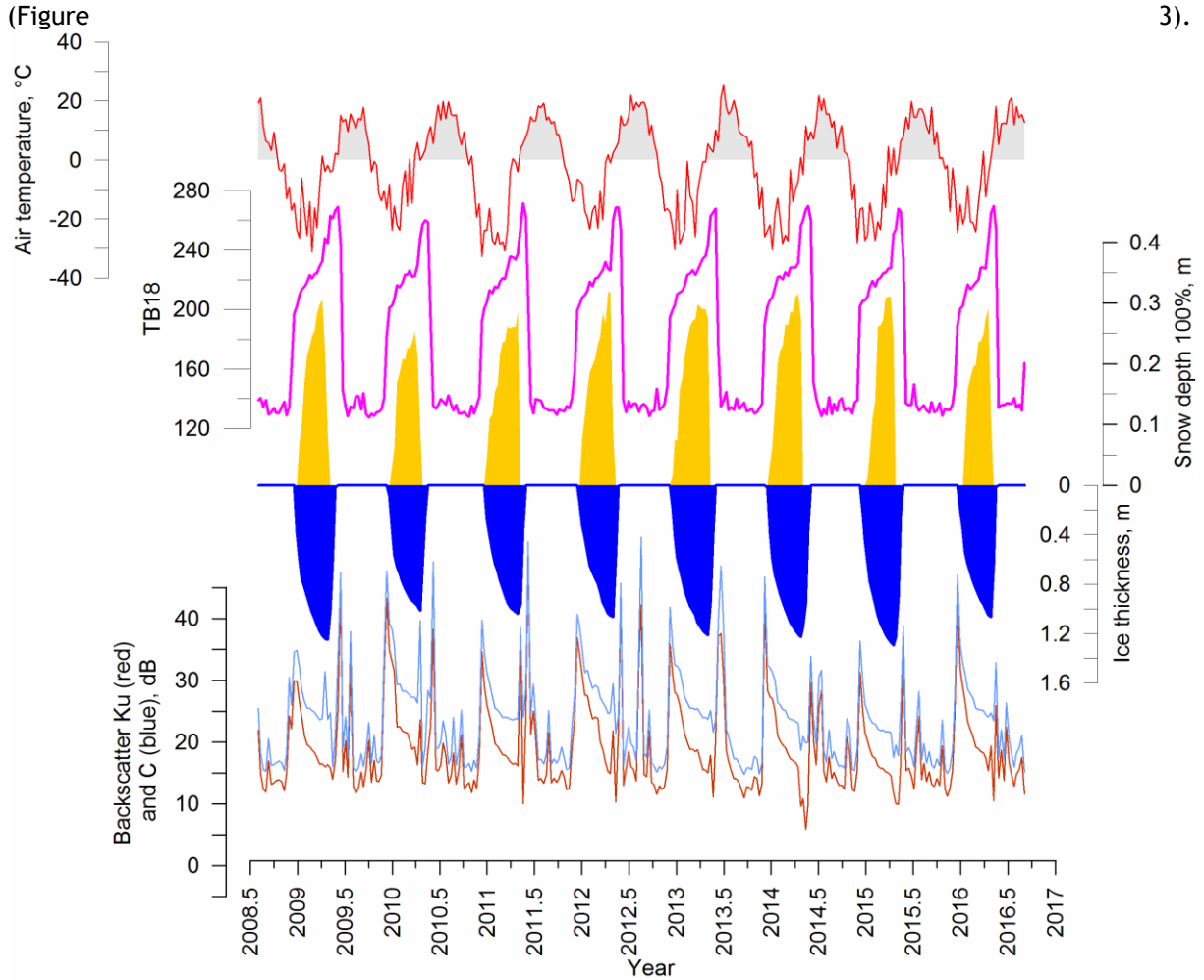


Figure 2. Temporal variability of ice thickness and snow depth as well as altimetry radar and radiometer measurements at the Great Slave Lake.

3.2. Algorithm Definition

The overall scheme of LIT retrievals is presented in Figure 3. The calibration step of the algorithm is based on in situ ice thickness measurements (if available) or simulated with the 1-D thermodynamic lake ice model CLiMo (Duguay et al., 2003). In the LIT production step, the algorithm uses the static calibrated parameters and ice flag initially obtained from the ice phenology dates module.

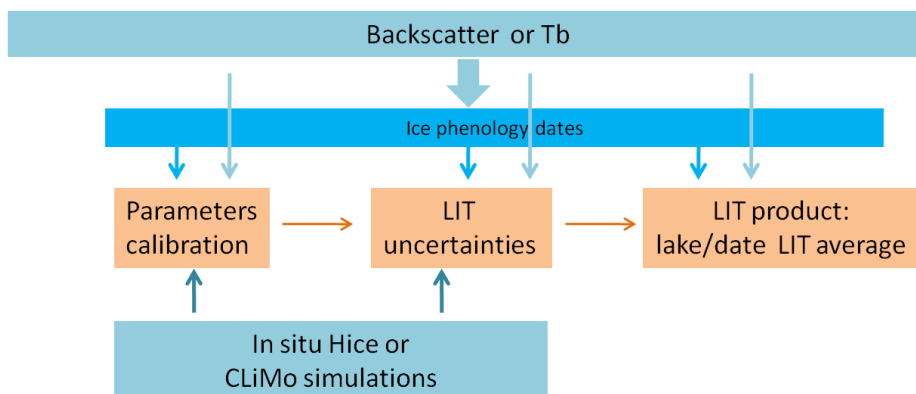


Figure 3. Major steps in LIT processing.

3.2.1. Ice phenology dates definition algorithm

The algorithm for lake ice phenology dates (LIPD) definition consists in the separation of water and ice clusters using two-dimensional σ_0 -TB/2 histograms and definition of an equation of a separation line (red line in Figure 2) passing through the minimum of the 2-D histogram. Linear equation (1) provides results with good accuracy (Kouraev et al., 2003, 2004, 2007a,b, 2008a,b, 2015; Kouraev, 2004). It has been shown that a specification of parameters in Equation (1) for each lake and for each satellite mission allows for lower uncertainties.

$$TB/2_{wi} = a * \sigma_0 + b \quad (1)$$

where $TB/2_{wi}$ is water/ice discrimination threshold, and a and b are parameters.

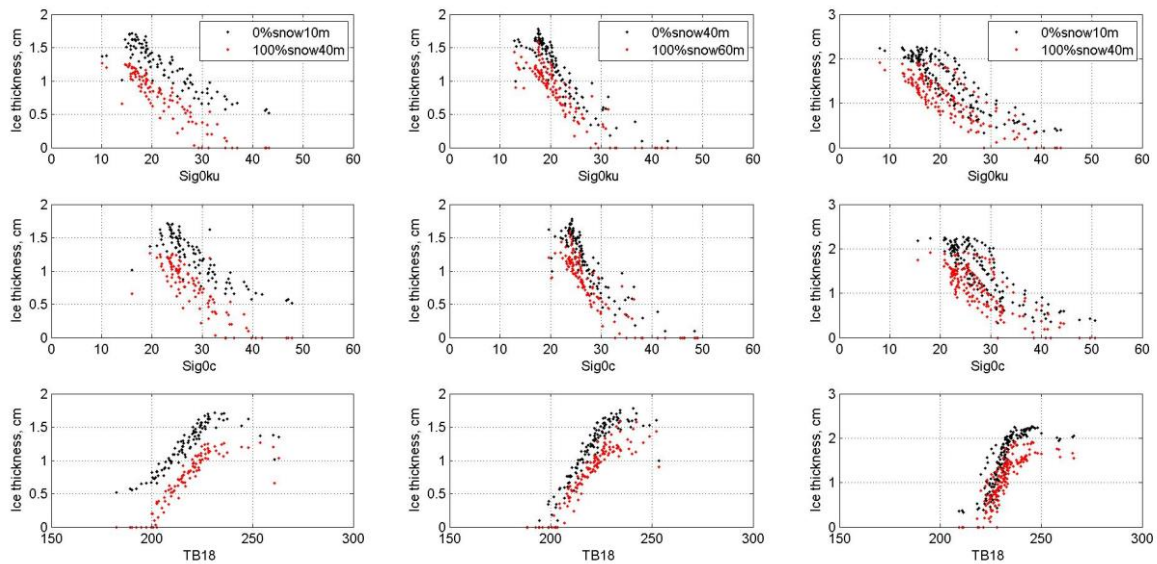
The water/ice flags are defined by comparing the $TB/2_j$ values for each cycle with $TB/2_{wi}$ values obtained from the Equation 1 and σ_0_j for the same cycle (Equation 2).

$$\begin{cases} \text{if } TB/2_j \leq TB/2_{wi}, \text{ Flag} = 0 \text{ (water)} \\ \text{if } TB/2_j > TB/2_{wi}, \text{ Flag} = 1 \text{ (ice)} \end{cases} \quad (2)$$

3.2.2. LIT retrieval

The LIT retrieval empirical module is based on functional relations between LIT and backscatter or LIT and brightness temperature (Figure 4). The relations are lake- and mission-specific and require the calibration of parameters. For Canadian lakes, calibration of the parameters is based on four years of simultaneous satellite measurements and CLIMo simulations. The selected years allow for characterisation of a variety of ice, snow-on-ice and weather conditions.

Geophysical characteristics affecting ice appearance and melt in near-shore areas, where in situ measurements are acquired, differ from that of in off-shore areas. As no ground measurements exist in off-shore areas, the CLIMo model is run with different scenarios of snow depth on ice and depth of lake water mixed layer (Duguay et al., 2003). The calibration of parameters for LIT_{CLIMo} - σ_0 and LIT_{CLIMo} - TB relations is run for LIT_{CLIMo} issued from different scenarios. The scenario that demonstrates the highest correlation and lowest LIT uncertainties is selected. This scenario is specific to each lake, as the amount of snow-on-ice and the lake mixing depth differ from lake to lake (Table 1). As the next step, the best scenario LIT_{CLIMo} - σ_0 and LIT_{CLIMo} - TB relations is fitted with a first-order polynomial function.



(a) (b) (c)

Figure 4. Relation between altimetric and radiometric measurements and modelled ice thickness for two extreme scenarios of on-ice snow depth and lake mixed-layer depth for (a) Great Slave Lake, (b) Great Bear Lake, and (c) Baker Lake (Canada).

Table 1. An example of the best-fit CLIMo scenarios used with Jason-2 altimetric and radiometric measurements. Snow depth is given in % from snow depth measured at local meteorological stations.

Lake name and Jason-2 track or track sub-part	CLIMo scenarios for σ_0 _Ku	CLIMo scenarios for TB18
Baker_Lake_Tr19	Snow (0%), mixing depth 30m	Snow (0%), mixing depth 10m
Great Bear_Tr225	Snow (0%), mixing depth 30m	Snow (0%), mixing depth 30m
Great Bear_Tr47	Snow (50%), mixing depth 40m	Snow (75%), mixing depth 30m
Great Slave_Tr254_South	Snow (50%), mixing depth 30m	Snow (0%), mixing depth 30m
Great Slave_Tr45_East	Snow (50%), mixing depth 30m	Snow (0%), mixing depth 30m

3.2.3. LIT retrievals editing

Studies using SARAL/AltiKa (Kouraev et al., 2015) and Jason-3 (Kouraev et al., 2021) altimeter data demonstrate that in early spring, when air temperatures are still mostly negative, lake snow can undergo metamorphism under the influence of solar radiation. At that time, a drop in backscatter in the order of 5-10 dB and small peak of TB measurement can be observed at all frequencies (Figure 5). This backscatter decrease and TB increase result in high LIT overestimation. As the pre-melting σ_0 drop/TB rise are not related to ice growth, the period of snow metamorphism needs to be removed from the processing. Since at this moment the difference between TB24 and TB18 (in the case of Jason-2) becomes close or above zero (Figure 5, low panel), the criteria $dTB_{24-18} \geq 0$ is used for identification of such cases and for corresponding detection and rejection of outliers in LIT output product.

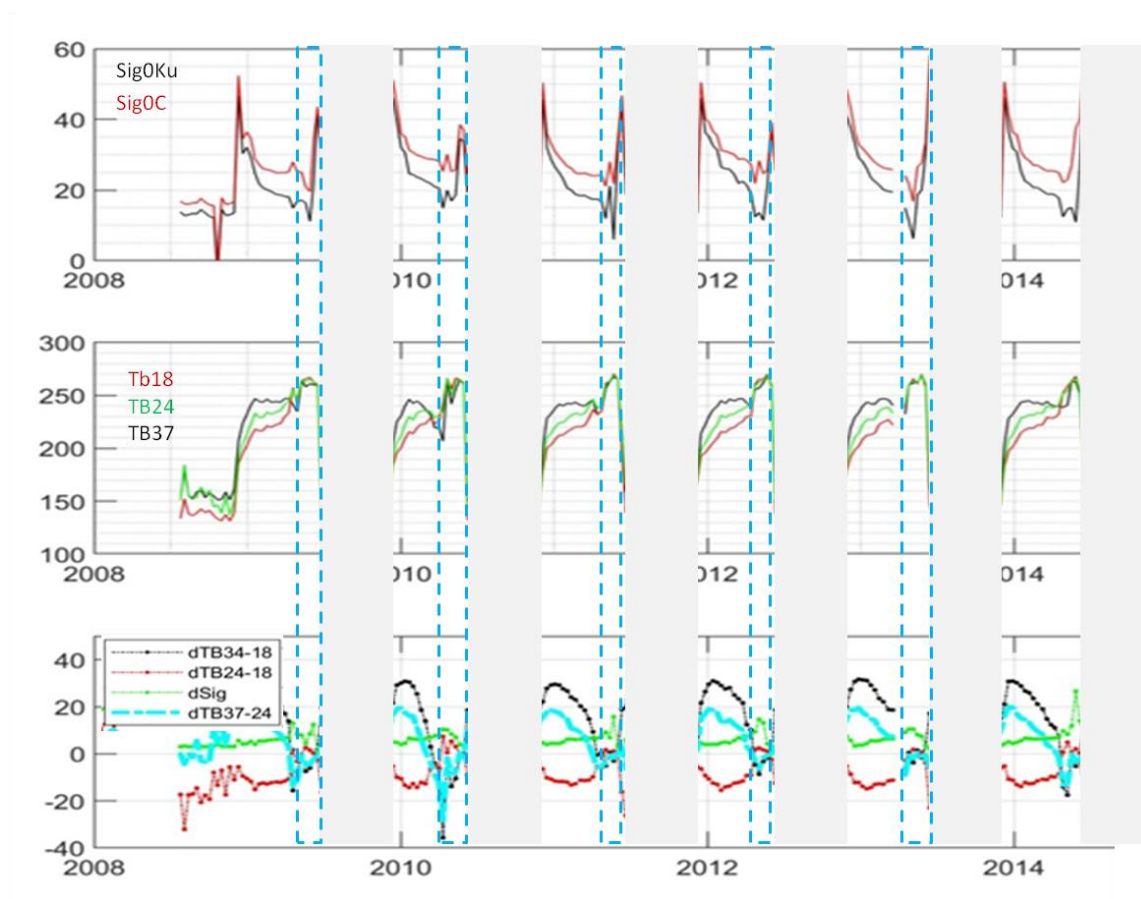


Figure 5. Winter changes of Jason-2 altimetric and radiometric measurements over the Great Slave Lake. Periods of snow pre-melt metamorphism are highlighted by blue dashed-line boxes.

3.3. Input Data

Input data for the empirical algorithm include backscatter measurements at Ku-band, brightness temperature measurements at 18 GHz, 24 GHz and 37/34 GHz, CLIMo LIT simulations and MODIS/Terra Corrected Reflectance True Color composite images. Satellite altimetry data are available via AVISO+ (<https://www.aviso.altimetry.fr>) portal and CTOH (<http://ctoh.legos.obs-mip.fr/data>) for Jason-2 and ENVISAT missions, respectively. The CLIMo LIT simulations are provided by H2O Geomatics. MODIS images for each lake are downloaded from NASA's WorldView data portal (<https://worldview.earthdata.nasa.gov/>). Detailed input data access description is provided in D1.2: Data Access Requirement Document (DARD).

3.3.1. Satellite altimeter backscatter measurements

Satellite altimeter backscatter measurements at Ku-band (13.6 GHz, wavelength 2.2 cm) retrieved with the ICE retracker are extracted from geophysical data records products (GDR) of ENVISAT and Jason-2 missions. The measurements are taken along satellite tracks with 20 Hz frequency and provide a spatial resolution of 300 m. Data are extracted using lake boundaries, excluding near-coastal buffer zones defined from MODIS images. The width of coastal zone buffers depends on satellite track/lake over-crossing length; equal to 20 km for large lakes and 10 km for narrow lakes.

3.3.2. Satellite altimeter brightness temperature measurements

Radiometer brightness temperature measurements at frequencies of 18.7 GHz, 23.8GHz and 36.5GHz/34.0GHz (ENVISAT/Jason) are extracted from geophysical data records products (GDR) of ENVISAT and Jason-2 missions. The measurements are done along satellite track with 1 Hz frequency. They are interpolated using a spline function to match 20 Hz radar measurements. Similar to backscatter measurements, the TB data are extracted using lake boundaries, excluding near-coastal buffer zones defined from MODIS images.

3.3.3. CLIMo LIT simulations

CLIMo LIT simulations represent daily ice thickness data for a combination of on-ice snow depth/mixing layer scenarios. The following range of scenarios is used for on-ice snow depth: 0%, 25%, 50% 75%, 100% and for lake mixed-layer depth: 10 m, 20 m, 30 m, 40 m, 50 m, and 60 m. On-ice snow depth represents the percentage of snow measured at a nearby local meteorological station (or atmospheric reanalysis data) on a given date.

3.3.1. MODIS/Terra Corrected Reflectance images

MODIS/Terra Corrected Reflectance True Color (Red = Band 1, Green = Band 4, Blue = Band 3) composite images extracted from MOD02QKM doi:10.5067/MODIS/MOD02QKM.061; MOD02HKM doi:10.5067/MODIS/MOD02HKM.061; MOD021KM doi:10.5067/MODIS/MOD021KM.061 product via WorldView portal (<https://worldview.earthdata.nasa.gov/>) are used as auxiliary data. They serve for the geographical selection of satellite altimeter measurements and definition of coastal buffer zones allowing to avoid or reduce (for narrow lakes) the effect of land contamination on radar and radiometric measurements.

3.4. Output Data

The structure of LIT output product from the empirical algorithm is presented in Table 2. Data will be provided in csv format.

Table 2. List of LIT product variables.

Variable name	Description	Units	Type	Dims
time	Time of measurement	decimal year	do	time
year	Year of measurement		do	time
month	Month of measurement		do	time
day	Day of measurement		do	time
lon	Lake center longitude [-180;+180]	degrees	do	time
lat	Lake center latitude [-90;+90]	degrees	do	time
LIT_sigKu	Ice thickness retrieved from Ku-band backscatter by empirical method [0; 3]	m	do	time

LIT_tb18	Ice thickness retrieved from brightness temperature measurements at 18 GHz frequency by empirical method [0; 3]	m	do	time
LIT_sigKu_std	Standard deviation of Ice thickness retrieved from Ku-band backscatter by empirical method for a given date [0; 3]	m	do	time
LIT_tb18_std	Standard deviation of Ice thickness retrieved from brightness temperature measurements at 18 GHz frequency by empirical method for a given date [0; 3]	m	do	time
mission	Satellite mission name used for LIT retrieval		char	time

3.5. Quality Assessment

Uncertainties of fitting as well as the errors in LIT retrievals are assessed using the mean absolute bias (Equation 3) and the root mean squared error (RMSE) (Equation 4) estimated between satellite-retrieved LIT and the LIT simulated by the model. Fitting errors are estimated for calibration period, while the LIT retrievals errors are evaluated on an independent dataset. Correlation coefficients are also provided.

$$Bias = \frac{\sum(LIT_{cliMo} - LIT_{sat})}{N} \quad (3)$$

$$RMSE = \sqrt{\frac{\sum(LIT_{cliMo} - LIT_{sat})^2}{N}}, \quad (4)$$

where LIT_{cliMo} and LIT_{sat} are modelled and satellite-retrieved ice thickness, respectively, and N is number of retrievals.

4. Algorithm Based on Radar Waveforms

This section describes the algorithm for the Lake Ice Thickness (LIT) production chain based on the exploitation of altimeter waveforms (Low Resolution Mode) that contain information correlated with the seasonal evolution of ice thickness over freshwater lakes. A detailed description of the algorithm and results are provided in Mangilli et al. (in preparation).

4.1. Modelling of the LIT signal in radar waveforms

The radar waveforms from altimetry missions show a specific signature on ice covered lakes. For LRM waveforms, this signature corresponds to a step-like break in the leading edge. This break is understood as the double back-scattering of the radar wave at 1) the snow-ice interface and at 2) the ice-water interface. The width of the step in the leading edge is directly related to the ice thickness. When the waveforms, measured along track each ~50 milliseconds (~350 meters), are lined up into a radar echogram, the step-like feature associated with the LIT translates into a distinguishable fringe, as shown in Figure 6.

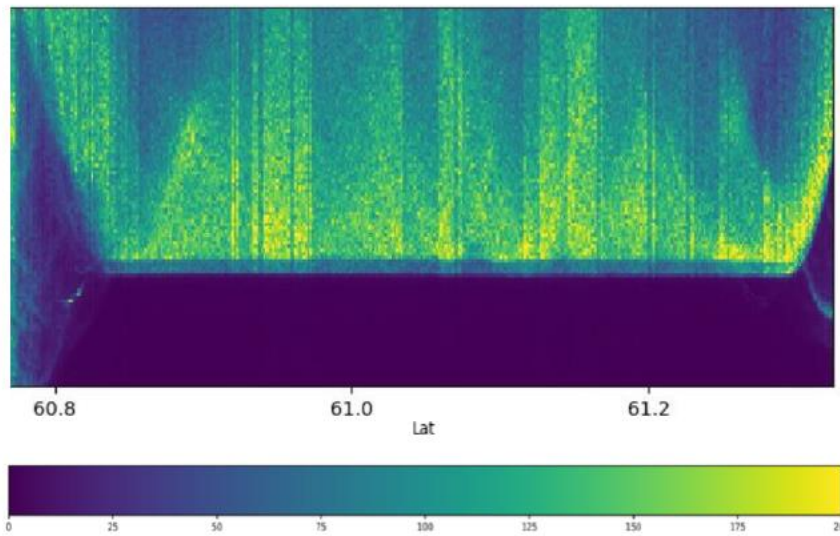


Figure 6. Example of LRM radar echogram over the iced-covered Great Slave Lake. Jason-3 data (pass 45, cycle 148, February 2020).

Given the specific signature of the LIT in radar LRM echograms, a physical model can be constructed, based on Brown's modelling of the radar echoes over an ocean surface, where the waveform is described as the sum of two backscattered echoes. The radar waveform, as a function of the range gates, $S(x)$, can therefore be defined as the sum of two positive definite error functions:

$$\begin{aligned} S_1(x) &= \text{erf}(x - x_c) + 1 \\ S_2(x) &= \text{erf}(x - x_c - \Delta_{ICE}^{gates}) + 1 \end{aligned} \quad (5)$$

where x is the range gates array of N gates samples, $\text{erf}(z)$ is the error function:

$$\text{erf}(z) = \frac{2}{\sqrt{\pi}} \int_0^z e^{-t^2} dt \quad (6)$$

x_c is the central gate of the first echo and Δ_{ICE}^{gates} is the ice thickness expressed in number of gates, that is, the width of the step in the leading edge. The modelled waveform takes the form:

$$S(x) = [S_1(x) + \alpha S_2(x)] e^{-\xi x} + N_t, \quad (7)$$

where $\alpha = [0, 1]$ is the amplitude of the second echo, ξ is the parameter associated to the attenuation of the second plateau, \hat{x} is the normalized samples vector, and N_t is the term associated to the thermal noise. The normalized waveform re-scaled by the overall amplitude A_{wf} , can therefore be modelled as:

$$S_{iced_lake}(x, \theta_p) = A_{wf} \hat{S}(x) \quad (8)$$

where $\hat{S}(x)$ is the model function of Eq. (4) normalized to unit and

$$\theta_p = \{A_{wf}, \Delta_{ICE}^{gates}, \alpha, \xi, x_c\} \quad (9)$$

is the five parameters vector. The ice thickness in unit of meters, Δ_{ICE} , is defined by applying the following conversion from range gates to meters:

$$\Delta_{ICE} = \Delta_{ICE}^{gates} \frac{c_{ice}}{2B} = \Delta_{ICE}^{gates} \frac{c}{n_{ice} 2B} \quad (10)$$

where B is the radar bandwidth, $c_{ice} = c / n_{ice}$ is the light speed in the ice, with c the speed of light in the vacuum and n_{ice} the refractive index of ice.

4.2. Algorithm Definition

The LRM LIT algorithm is a retracker specific to the LIT analysis of the radar waveforms, based on the modelling described in section 4.1. For each data cycle, and a given analysis window defined by a latitude cut $LW_{LIT} = [lat_{min}, lat_{max}]$ over a given target lake, the LIT analysis consists of two steps: 1) the optimization step, that is, the waveform fit, and 2) the estimation of the parameters' mean and standard deviation, as described below and summarized in Figure 7.

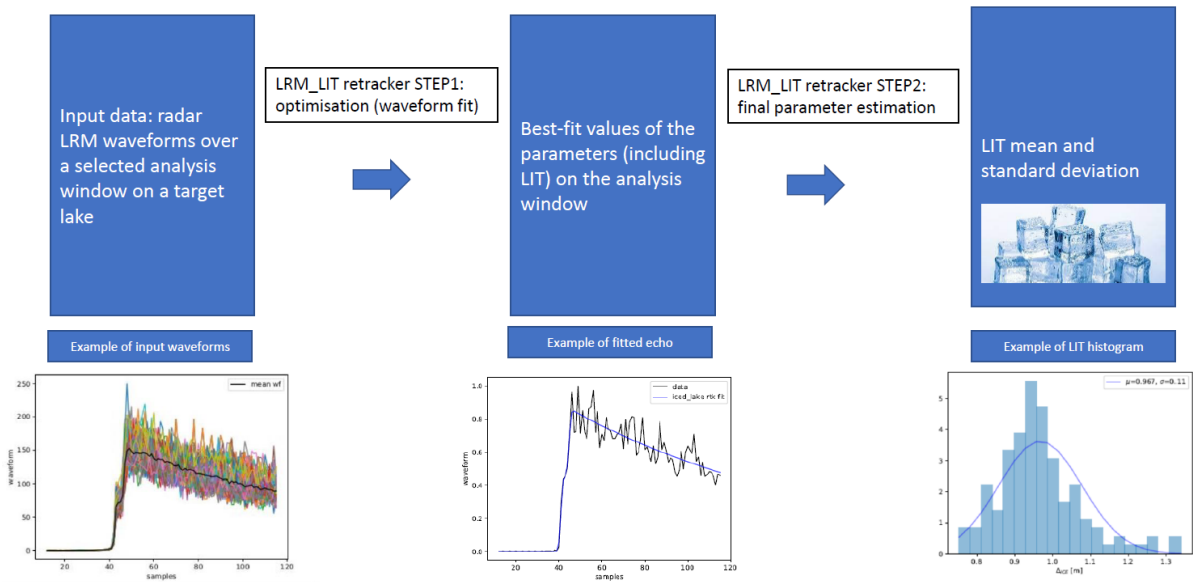


Figure 7. Major steps in LIT processing.

4.2.1. Step 1: Optimisation and best fit parameters

The optimisation step consists of performing a Least Square Levenberg-Marquardt weighted fit of each echo in the LIT analysis window with the model described in Sect. 4.1. The optimized function is:

$$\chi^2 = \mathbf{r}^T \mathbf{C}^{-1} \mathbf{r} \simeq \sum_i \left(\frac{r_i}{\sigma_i} \right)^2 \quad (11)$$

where, $\mathbf{r} = \mathbf{y}(x) - S_{\text{model}}(x; \theta_p)$ is the vector of residuals between the waveform data, $\mathbf{y}(x)$, and the model, $S_{\text{model}}(x; \theta_p)$. The weights, σ_i , are computed as the standard deviation of the echoes within the LIT analysis window. For each data cycle, a set of best fit values for each of the five parameters is provided from the fit of the individual echoes in the analysis window.

4.2.2. Step 2: Parameters estimation and LIT retrieval

The second step of the retracking analysis is the parameter estimation which provides, as the main output, the LIT measurement with the associated uncertainty. The estimation is done by computing the mean and standard deviation of the best fit parameters for each data cycle in the LIT analysis window. To get the constraints on the five parameters with the corresponding uncertainties for each cycle, the histograms of the five parameters best fit values estimated from the fit of each echo is computed. A Gaussian fit on the histograms is performed to get, for each parameter, the mean and variance.

In order to manage eventual outliers, we consider the fit results for which the model and the observations agree within three standard deviations (that is, a reduced chi-squared < 3). We also discard fit results that could give unrealistic LIT values of $\Delta_{\text{ICE}} > 3$ meters before computing the LIT histograms and performing the Gaussian fit.

4.2.3. Quality checks

We perform reduced chi-squared goodness of fit tests. An example of LIT estimation as a function of latitude along a Jason-2 altimeter track (step 1 of the LRM_LIT retracker) with the reduced chi-squared values for each fitted waveform over Great Slave Lake is shown in Figure 8. Reduced chi-squared values around 1 indicate that the fit performs correctly.

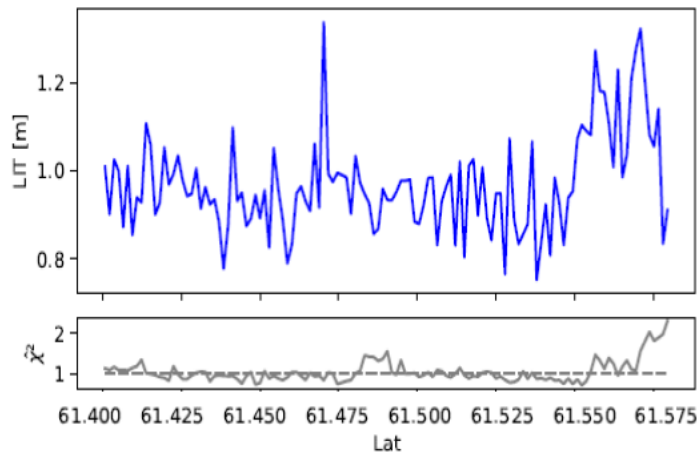


Figure 8. Example of LIT estimation as a function of the latitude along Jason-2 track 45 over the Great Slave Lake (Mangilli et al., in preparation).

4.3. Input Data

4.3.1. Input 1

For each data cycle and pass over a target lake, the input for Step 1 are the radar waveforms in the LIT analysis window.

4.3.2. Input 2

For each data cycle and pass over a target lake, the input for Step 2 are the best fit values of the five parameters for each fitted echo in the analysis window (that is the output of Step 1).

4.4. Output Data

The output data product contains:

- Main outputs (Step 2 output): LIT mean and standard deviation within the analysis window.
- Complementary outputs (Step 1 output): the best fit LIT estimations from the fit of each radar waveform in the LIT analysis window over the target lake with the corresponding coordinates. This typically consists of a ~100 LIT estimations for each cycle. It is useful to have this output to check the spatial evolution of the LIT in the analysis window and to eventually extract LIT estimates from a smaller region in the analysis window.

4.5. Validation and Quality Assessment

The LRM_LIT retracker has been validated on simulations representative of Jason-like missions. A summary is given in Figure 9, where the top plots refer to winter-like simulated waveforms (left panel) and the LIT histogram (right panel).

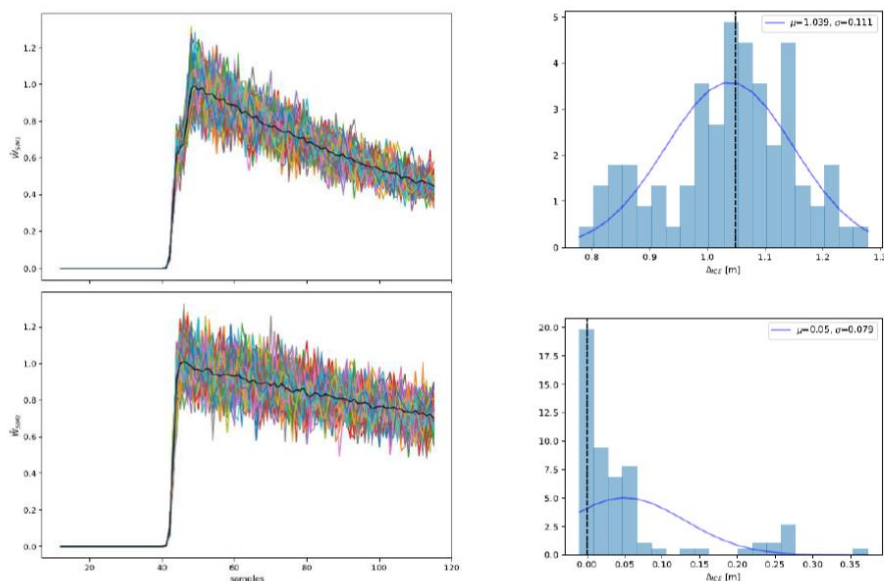


Figure 9. Summary of validation tests on Jason-like simulations (Mangilli et al., in preparation).

The input value used to generate the simulations is shown as a dashed line. The same description applies to the bottom plots, for the summer-like simulations without the ice signature. In both cases the LRM_LIT retracker gives unbiased LIT results with an uncertainty of ~10 cm.

LIT retrievals from satellite missions have been evaluated against LIT simulations from the thermodynamic lake ice model CLIMo (described in Sec. 2.2.3). A qualitative comparison with in-situ data was also performed when possible¹. Figure 10 provides an example of the comparison of the LIT estimations obtained within a winter season over Great Slave Lake with the LRM_LIT retracker applied to Jason-2 data (blue triangles) and Jason-3 data (red stars) and LIT from CLIMo (Duguay et al., 2003) simulations with different on-ice snow depth scenarios (diamonds) and in situ data (circles). There is an excellent agreement between Jason-2 and Jason-3 LIT estimates, which are fully compatible with the thermodynamic simulations and qualitatively in agreement with in situ data. We note that, in general, the LIT melting phase is detected earlier with the satellite-based measurements because of snow melting that perturbs the radar echoes.

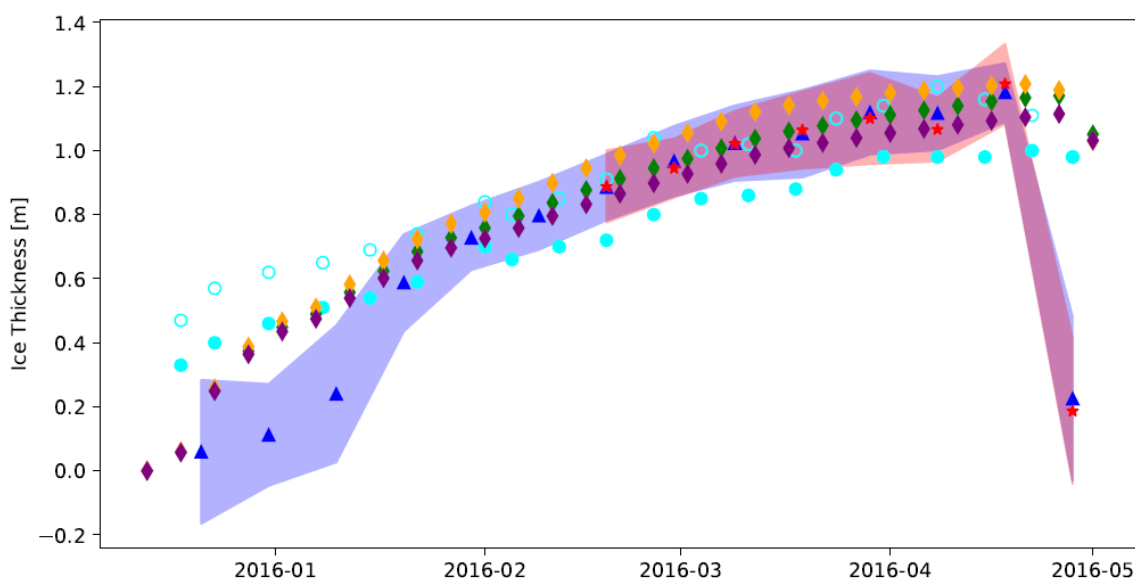


Figure 10. Example of the comparison of LIT estimates over the Great Slave Lake for one winter season (2015-2016): Jason-2 data (blue triangles), Jason-3 data (red stars), LIT from CLIMo simulations with different on-ice snow depth scenarios (diamonds) and in situ data (circles) (Mangilli et al., in preparation).

For a quantitative comparison between LIT estimates, the same metrics described in Sec. 2.4 are used, that is the Mean Bias Error (MBE) and the Root Mean Square Error (RMSE).

The LRM_LIT retracker provides consistent LIT estimates with an accuracy of the order of 10 cm and has the capability of capturing the LIT seasonal transitions (ice formation and melt) and the LIT inter-seasonal variations. It is therefore a powerful tool for LIT trend studies and monitoring.

¹ It is worth noting that the comparison between LIT estimates from satellite missions and in situ data must be taken with caution. In fact, in situ data are collected near the shore, while satellite data are taken from the middle of the lake to avoid land contamination. These are indeed two different environments in terms of bathymetry, wind exposure, snow type and quantity. All these parameters play a key role on ice formation and thickness and they can lead to significant LIT differences.

5. References

- Brown, L.C. & Duguay, C.R. (2010). The response and role of ice cover in lake-climate interactions. *Progress in Physical Geography*, 34(5), 671-704, doi: 10.1177/0309133310375653
- Brown, L.C. & Duguay, C.R. (2011). A comparison of simulated and measured lake ice thickness using a shallow water ice profiler. *Hydrological Processes*, 25, 2932-2941, doi: 10.1002/hyp.8087.
- Duguay, C.R., Zakharova, E.A., Kouraev, A.V., Kheyrollah Pour, H. & Hoekstra, M. (2018). Retrieval of ice thickness on large northern lakes from Jason-2 data, POLAR2018: Abstract Proceedings, Open Science Conference, Davos, Switzerland, 19-23 June, Abstract No. 2638, p. 46.
- Duguay, C.R., Flato, G.M., Jeffries, M.O., Ménard, P., Morris, K. & Rouse, W.R. (2003). Ice cover variability on shallow lakes at high latitudes: Model simulations and observations. *Hydrological Processes*, 17(17), 3465-3483.
- Ghiasi, Y., Duguay, C.R., Murfitt, J., Thompson, A., van der Sanden, J., Drouin, H. & Prévost, C. (2020). Application of GNSS interferometric reflectometry for the estimation of lake ice thickness. *Remote Sensing*, 12, 2721, doi:10.3390/rs12172721.
- Kheyrollah Pour, H., Duguay, C.R., Scott, A. & Kang, K.-K. (2017). Improvement of lake ice thickness retrieval from MODIS satellite data using a thermodynamic model. *IEEE Transactions on Geoscience and Remote Sensing*, 55(10), 5956-5965, doi: 10.1109/TGRS.2017.2718533.
- Kouraev, A.V., Papa, F., Buharizin, P.I., Cazenave, A., Crétaux, J.-F., Dozortseva, J. & Rémy, F. (2003). Ice cover variability in the Caspian and Aral seas from active and passive satellite microwave data. *Polar Research*, 22(1), 43-50.
- Kouraev, A.V., Papa, F., Mognard, N.M., Buharizin, P.I., Cazenave, A., Crétaux, J.-F., Dozortseva, J. & Rémy, F. (2004). Sea ice cover in the Caspian and Aral seas from historical and satellite data. *Journal of Marine Systems*, 47, 89-100.
- Kouraev, A.V. (2004). Synergy of active and passive satellite microwave data for the study of first-year sea ice in the Caspian and Aral seas. *IEEE Transactions on Geoscience and Remote Sensing*, 42(10), 2170-2176.
- Kouraev, A.V., Semovski, S.V., Shimaraev, M.N., Mognard, N.M., Legrésy, B. & Rémy, F. (2007a). Ice regime of Lake Baikal from historical and satellite data: Influence of thermal and dynamic factors. *Limnology and Oceanography*, 52(3), 1268-1286.
- Kouraev, A.V., Semovski, S.V., Shimaraev, M.N., Mognard, N.M., Legrésy, B., & Rémy, F. (2007b) Observations of lake Baikal ice from satellite altimetry and radiometry. *Remote Sensing of Environment*, 108, 240-253.
- Kouraev, A.V., Shimaraev, M.N., Buharizin, P.I., Naumenko, M.A., Crétaux, J.-F., Mognard, N.M., Legrésy, B. & Rémy, F. (2008a). Ice and snow cover of continental water bodies from simultaneous radar altimetry and radiometry observations. *Survey in Geophysics* 29(4-5): 271-295.
- Kouraev, A.V., Kostianoy, A.G. & Lebedev, S.A. (2008b). Recent changes of sea level and ice cover in the Aral Sea derived from satellite data (1992-2006). *Journal of Marine Systems*, 76(3), 272-280.
- Kouraev, A.V., Zakharova, E.A., Rémy, F. & Suknev, A.Y. (2015). Study of Lake Baikal ice cover from radar altimetry and in situ observations, *Marine Geodesy*, 38 (sup1), 477-486, doi.org/10.1080/01490419.2015.1008155
- Kouraev, A.V., Zakharova, E.A., Kostianoy, A.G., Shimaraev, M.N., Desinov, L.V., Petrov, E.A., Hall, N.M. J., Rémy, F. & Suknev, A. Ya. (2021). Giant ice rings in Southern Baikal: multi-satellite data help to study ice cover evolution and eddies under ice, *The Cryosphere Discuss.* [preprint], <https://doi.org/10.5194/tc-2021-146>, in review/accepted.
- Legrésy, B. & Rémy, F. (1997). Surface characteristics of the Antarctic ice sheet and altimetric observations, *Journal of Glaciology*, 43(14), 265-275, doi.org/10.3189/S002214300000321X.
- Mangilli, A., Thibaut, P., Duguay, C.R. & Murfitt, J. (in preparation). A new approach for the estimation of the lake ice thickness from conventional radar altimetry. To be submitted to *IEEE Transactions on Geoscience and Remote Sensing*.

Murfitt, J.C., Brown, L.C. & Howell, S.E.L. (2018). Estimating lake ice thickness in Central Ontario. PLoS ONE, 13(12), e0208519, <https://doi.org/10.1371/journal.pone.0208519>.

Murfitt, J. & Duguay, C.R. (2021). 50 years of lake ice research from active microwave remote sensing: Progress and prospects. Remote Sensing of Environment, 264, 112616, <https://doi.org/10.1016/j.rse.2021.112616>.

Surdu, C., Duguay, C.R., Brown, L.C. & Fernández Prieto, D. (2014). Response of ice cover on shallow Arctic lakes of the North Slope of Alaska to contemporary climate conditions (1950-2011): Radar remote sensing and numerical modeling data analysis. The Cryosphere, 8, 167-180, doi:10.5194/tc-8-167-2014.

Vuglinsky, V. (2017). Assessment of changes in ice regime characteristics of Russian lakes and rivers under current climate conditions. Natural Resources, 8, 416-431.

Zakharova, E., Agafonova, S., Duguay, C., Frolova, F. & Kouraev A. (2020). River ice phenology and thickness from satellite altimetry. Potential for ice bridge road operation. The Cryosphere Discussions, 2020/12/16, 1-31.